



A study of radicals in industrial raw cristobalite powders

Francesco Di Benedetto¹ · Andrea Giaccherini² · Maurizio Romanelli¹ · Giordano Montegrossi³ · Elena Belluso^{4,5} · Silvana Capella^{4,5} · Alfonso Zoleo⁶ · Giulio Arcangeli⁷ · Alessandro Marinaccio⁸ · Ottorino Gottardo⁹ · Fabio Capacci¹⁰

Received: 28 July 2020 / Accepted: 26 November 2020 / Published online: 4 February 2021
© The Author(s) 2021

Abstract

We report the results of an experimental multianalytical characterisation of industrial cristobalite powders, used as raw materials for artificial stone production. Cristobalite is considered a serious threat to human health. The study was carried out through X-ray diffraction (XRD), scanning electron microscopy with energy dispersive microanalysis (SEM/EDS), continuous-wave (cw) and pulse electron paramagnetic resonance (EPR) spectroscopy. Our results point out a sub-micrometric size of the structural coherence in cristobalite, associated with numerous stacking defects. Moreover, the material was found characterised by the presence of superoxide radicals, whose persistence appears conceivably long. Radicals in a material synthesized through a high-temperature treatment were generated during the grinding step in the industrial production of cristobalite. During this process, in fact, both superoxide generation and structural defectivity are induced. Indeed, cristobalite powders already result activated by a radical population, before any kind of process in artificial stone production.

Keywords Cristobalite · Crystalline silica · Industrial production · EPR spectroscopy · Toxicity

Introduction

Among the numerous polymorphs of the crystalline silica, SiO₂, cristobalite (CAS no. 14464-46-1) deserves a relevant attention in the context of occupational exposure, being rated as “carcinogenic to humans” by the IARC (2012). Based on experimental studies, cristobalite resulted associated with a fibrogenic potential higher than that of α -quartz (ACGIH 2010; Park et al. 2002). Accordingly, the Threshold Limit Values (TLV) for crystalline silica resulted occasionally split in specific values for α -quartz and cristobalite (Andersson et al. 2008). In US, OSHA reduced to 0.05 mg/m³ the TLV for the respirable fractions of all crystalline silica polymorphs. In EU, Belgium France, Spain and Sweden adopted a TLV of 0.05 mg/m³ for cristobalite versus that of 0.1 mg/m³ for α -quartz. The EU in its 2398/17 adopted the carcinogenicity of crystalline silica while setting the TLV at 0.1 mg/m³. Nonetheless, the TLV fixed by EU directive seems only partially adequate to the carcinogenic power of crystalline silica, and to the risk associated to exposure, even at low doses, to cristobalite. Clusters of workers exhibiting silicosis have been found, in the last years, in the production of microcasted gold (Murgia et al. 2007; Romanelli et al. 2012) and of artificial stone (Di Benedetto et al. 2019; Leso

✉ Francesco Di Benedetto
francesco.dibenedetto@unifi.it

- ¹ Dipartimento di Scienze della Terra, Università degli Studi di Firenze, Florence, Italy
- ² Dipartimento di Ingegneria Industriale, Università degli Studi di Firenze, Florence, Italy
- ³ Istituto di Geoscienze e Georisorse (CNR-IGG), Florence, Italy
- ⁴ Dipartimento di Scienze della Terra, Università Degli Studi Di Torino, Turin, Italy
- ⁵ Centro Interdipartimentale per lo studio degli Asbesti e di altri Particolati Nocivi “G. Scansetti”, Università Degli Studi Di Torino, Turin, Italy
- ⁶ Dipartimento di Scienze Chimiche, Università di Padova, Padua, Italy
- ⁷ Dipartimento di Medicina Sperimentale e Clinica, Università degli Studi di Firenze, Florence, Italy
- ⁸ INAIL, Laboratorio di Epidemiologia Occupazionale ed Ambientale, Rome, Italy
- ⁹ Azienda ULSS, 6 Euganea, Padua, Italy
- ¹⁰ Azienda USL Toscana Centro, Florence, Italy

et al. 2019) and among the dental technologists (Barbieri et al. 2020).

Apart from quartz, cristobalite is the second most abundant polymorph on the Earth's crust, and the only polymorph, still but quartz, object of a relevant diffusion in the industrial production (MAK 2012). The main industrial applications of cristobalite conventionally span from abrasives to pigments, to metal casting, to the production of chemicals. Recently, cristobalite was described also in some products belonging to the so-called artificial stone composite materials, which are mixtures of silica minerals and polyester or acrylic resins (Di Benedetto et al. 2019). Besides its use as the main constituent of a material, cristobalite is virtually present in almost all quartz-bearing production, due to its mineralogical affinity in some natural settings (most of the industrial silica has a natural origin, USGS 2016), although in concentrations rarely exceeding 1 wt% (IARC 2012). Studies were carried out also on volcanic ashes, where cristobalite is a common constituent of andesitic lavas (Horwell et al. 2003).

Numerous studies (e.g. Fubini et al. 1990, 1999; Daniel et al. 1995; Sugiyama et al. 1998) were devoted to the investigation of the chemical and structural causes of cristobalite toxicity to humans, supposedly very similar to that exploited by α -quartz. Namely, radicals or dangling bonds, associated to the formation of a fresh fracture, were considered relevant for toxicity issues (Fubini et al. 1990, 1999). These radicals were described as able to interact with air and especially moisture, to form oxidised and peroxidised species (Fubini et al. 1990, 1999; Musso et al. 2010; Giordano et al. 2007). Moreover, these radicals are also characterised by a relatively long lifetime (Fubini et al. 1990).

The present study is aimed to extend the literature's findings with the identification and characterisation of the radical speciation of industrial cristobalite powders used as raw materials in the production of the artificial stone. The production of cristobalite-containing material (slabs) is increasing in various parts of the world owing to many useful properties as e.g. the low water absorption, low porosity and high abrasion resistance. Since several manufacturing steps implicate the air dispersion of respirable particles and since these last are considered highly toxic (IARC 2012), for the risk evaluation and for the assurance purposes (Leso et al. 2019) a complete chemico-physical characterization is compulsory. The sample here considered belongs to a filler (a material characterised by a high fraction of respirable particles) and it is analysed without any kind of pre-treatment. The mineralogical, chemical and morphological characterisation of the investigated industrial sample was carried out through XRD and SEM/EDS, respectively. FTIR measurements were included to verify the eventual presence of water in the sample. The radical population in the sample was identified and characterised through EPR spectroscopy

(both in the cw and pulse modes). EPR (electron paramagnetic resonance) is a technique devoted to studying paramagnetic species, i.e. chemical species with unpaired electrons like radicals and many transition ions and defects in crystals. EPR can highlight structure and features of a paramagnetic centre probing the interactions of the centre with close magnetic nuclei (like ^1H , ^{14}N , ^{13}C). Very small interactions with close nuclei, which cannot be detected in cw-EPR (continuous wave EPR), can be revealed through a pulsed EPR technique like ESEEM (Electron Spin Echo Envelope Modulation).

Materials and methods

Materials

The investigated powders consist of microcrystalline powders with a very fine granulometry (nominally $< 4 \mu\text{m}$). These mixtures are modelled in various shapes (essentially for countertop and bathroom furniture's production), the resins are let harden, and the final object is polished as a natural stone. The seldom presence of cristobalite, in spite of quartz, in the production of silica-based artificial stone has been firstly described by Di Benedetto et al. (2019).

X-ray powder diffraction

XRPD patterns of the investigated samples were performed using a Bruker New D8 Da Vinci powder diffractometer and employing Ni-filtered $\text{Cu K}\alpha$ (1.54187 \AA) radiation. XRPD patterns were registered at 1,600 W (40 kV, 40 mA) with a fast multi-channel detector in the 2θ range $3\text{--}80^\circ$, applying a step size of $0.03^\circ 2\theta$. The qualitative identification of the main mineralogical phases present in the samples was accomplished through the QualX2 software, operating over the PDF-2 and POW-COD databases (Altomare et al. 2015). Crystallite dimension was established by means of the hkl-phase routine implemented in the Topas 4.2 software, provided by Bruker AXS Inc. (Madison, Wisconsin, USA). This routine fits the peaks with pseudo-Voigt functions on all the peaks disregarding any structural model. The peak profiles are related to the crystallite size and strain.

Scanning electron microscopy

Three aliquots of the sample were placed on stubs using double-sided conductive adhesive tape and coated with graphite. Secondary electron micrographs were obtained using a SEM ZEISS EVO MA15 with accelerating voltage of 20 kV. Energy Dispersive (EDS) microanalytical investigation was obtained through an INCA 250 Oxford mounted in the above-mentioned microscope. The peaks were fitted

by Gaussian curves applying the ZAF (atomic number, absorption, fluorescence) correction.

Fourier transform infrared spectroscopy

The characterisation of the sample through Fourier Transform InfraRed spectroscopy (FTIR) was carried out by means of a Perkin Elmer Spectrum 100 instrumentation, available at the Department of Earth Sciences of the University of Florence. The spectra were registered in the Attenuated Total Reflectance (ATR) mode, using the Universal ATR accessory mounted on the main instrumentation. Spectra were registered in the range 4000–380 cm^{-1} , with a step size of 1 cm^{-1} .

EPR spectroscopy

Conventional EPR spectra of the sample powders, inserted in amorphous silica tubes using a Teflon bag, were registered at room temperature using a Bruker ER 200D-SRC spectrometer (Dept. of Chemistry, Univ. of Florence). The spectrometer operates at X-band (~ 9.5 GHz), interfaced with DS/EPR software to a PC for data acquisition and handling. Operating conditions were 0.05 mT modulation amplitude and 100 kHz modulation frequency. Scan speed was set to 2.5 mT/s, and the investigated range 0–1 T.

Low-temperature EPR spectra have been also acquired at the Department of Chemical Sciences of the University of Padua by using a Bruker ELEXYS X-band EPR, equipped with an Oxford CF935 cryostat and a dielectric cavity with high Quality (Q) factor. The continuous wave cw-EPR measurements were carried out in a cryostat at 35 K. Spectra were registered in the magnetic field range 50–650 mT (panoramic spectra) and 320–360 mT (detailed spectra), with 0.05 mT modulation amplitude and 100 kHz modulation frequency. Nominal resolution and scan speed were set to 0.48 mT and to 5 $\text{mT}\cdot\text{s}^{-1}$, respectively, for the panoramic spectra, and to 0.02 mT and to 0.2 $\text{mT}\cdot\text{s}^{-1}$, respectively, for the detailed spectra.

Pulsed EPR investigations included the registration of both fields swept Echo-EPR (EEPR) and Electron Spin Echo (ESE) decays. All measurements were carried out at 35 K on the same Bruker ELEXYS X-band EPR. Echo-EPR spectra were registered after a two-pulse $\pi/2-\tau-\pi-\tau$ sequence at an operating frequency of ~ 9.70 GHz (1st and 2nd pulse lengths 16 and 32 ns, respectively, 200 ns interpulse time, operating frequency 9.7392(1) GHz). The magnetic field was varied in the range 300–360 mT. Time-domain ESE decays were registered after a three-pulse $\pi/2-\tau-\pi/2-T-\pi/2-\tau$ sequence (1st, 2nd, 3rd pulse length 16 ns, 1st and 2nd interpulse times 136 and 80 ns respectively, operating frequency 9.7393(1) GHz), setting the magnetic field at the value corresponding to the maximum intensity of the Echo-EPR

spectrum of the same sample. The experimental time domain was in the range 0–4096 ns, with a time step of 8 ns and a dead-time of 216 ns. Electron Spin Echo Envelope Modulation (ESEEM) patterns were extracted by subtracting a decay function obtained by refining a bi-exponential model. The resulting ESEEM pattern was Fourier transformed after Hanning windowing and zero-filling the raw data.

Results

X-ray powder diffraction and scanning electron microscopy

Chemical, phase composition, and morphology have been obtained by XRPD and SEM. The powder XRD pattern of the investigated cristobalite sample (Fig. 1a) shows no relevant amorphous fraction. The analysis reveals that cristobalite is the only species present in the XRD pattern (up to 99%). Only a very small peak attributable to quartz was revealed at $26.6^\circ 2\theta$. The detail of the pattern in the angular region close to the (101) reflection of cristobalite (inset to Fig. 1a) reveals features very frequently associated with opaline samples (Curtis et al. 2019) and attributed either to a poor long-range coherence in the crystal structure or to the presence of tridymite/cristobalite stacking sequences (Florke et al. 1991). Jones and Segnit (1971) and Florke et al. (1991) classified samples with features very close to those shown in Fig. 1a as “opal C”. This definition, falling in the wide classification of the opals, should imply the presence of some crystallisation water in the sample (Florke et al. 1991; Curtis et al. 2019). This issue will be reconsidered in the next paragraphs. The cristobalite peak widths are somehow large, suggesting a very small crystal size. The analysis of the line profile was carried out in the range between 25 and 80 2θ degrees (to avoid misinterpretation due to the presence of the above-discussed disorder-related features) and pointed out a mean crystallite dimension of 200(60) nm.

The representative sample micromorphology is shown in the Figs. 1b–d. Relatively large and irregular shaped particles (in the range 1–10 μm), coupled to very small ones (0.5–2 μm), are the main constituents of the whole micromorphology of the sample. At higher magnification, the big particles appear aggregates of smaller units, still in the range 0.5–2 μm . Small particles appear anhedral and do not exhibit a preferential habitus. When clustered, platy like aggregates are frequently observed. The average size of the two groups of particles are 4.01 μm and 0.69 μm , respectively.

The chemical composition of the sample, investigated by means of EDS microanalyses, carried out both in the punctual and raster modes, is homogeneous throughout the sample (within the EDS accuracy limits). Mean chemical composition of Na, Al, Si and O, equal to 0.30, 0.22,

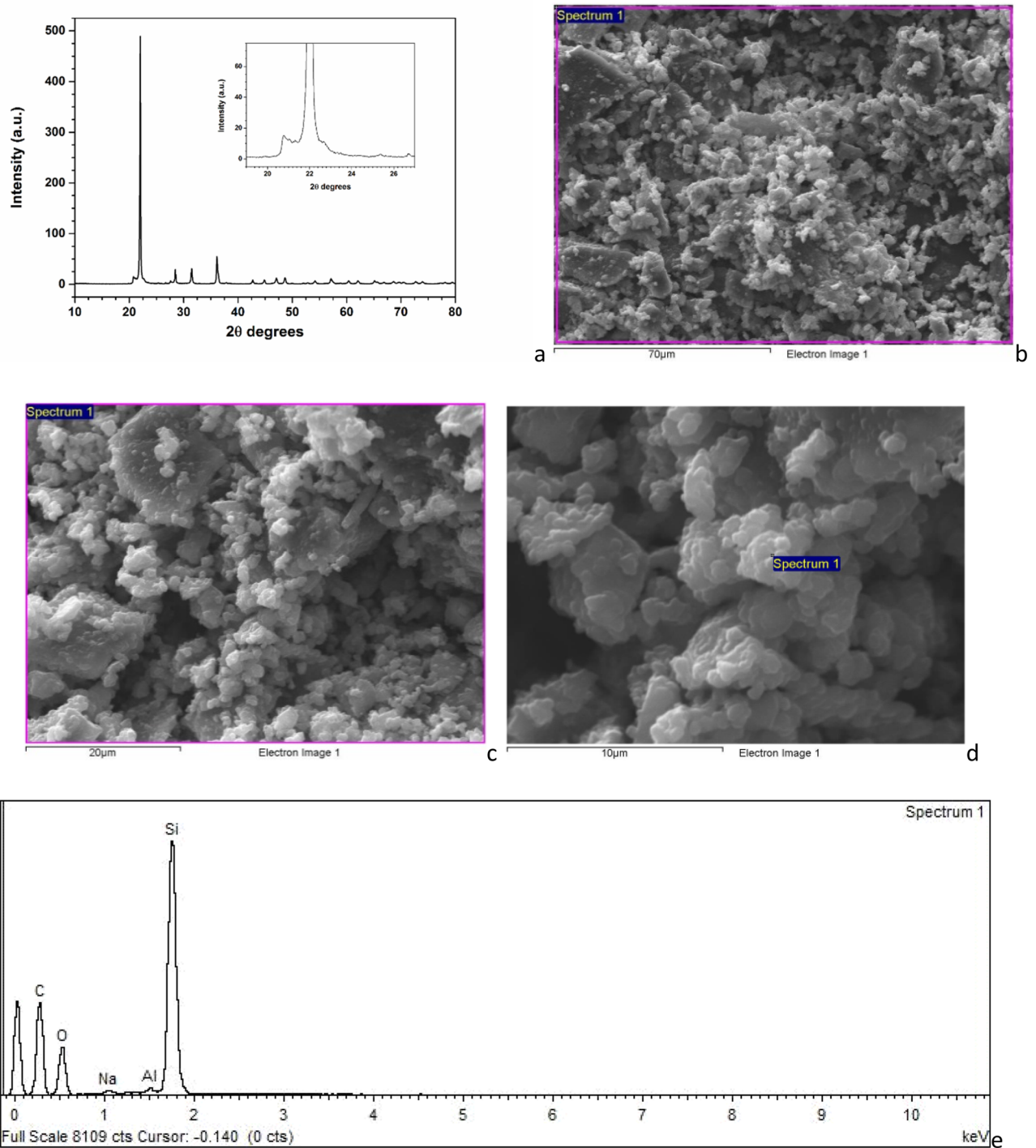


Fig. 1 a XRD pattern of the investigated sample. In the inset, detail of the low intensity features around the main (101) reflection of cristobalite. Secondary electron micrographs (b 360X, c 1000X, d 11700X); e EDX spectrum representative of the sample

33.0 and 66.48 at%, respectively, was evaluated (Fig. 1e). This composition can be explained in terms of SiO_2 and a

minor quantity (<3 wt%) of albite, $\text{NaAlSi}_3\text{O}_8$. This latter phase occurs in a very low amount and thus at the order of

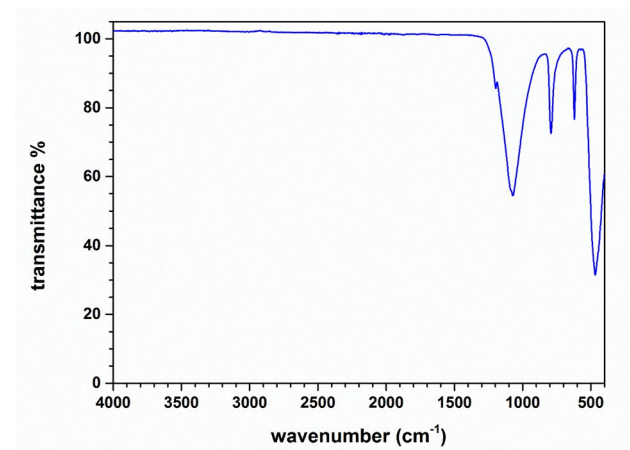


Fig. 2 FTIR spectrum of the investigated sample

the detection limit of the XRD characterisation (especially considering the high linewidth values).

FTIR

The FTIR spectrum of the investigated sample (Fig. 2) reveals features fully compatible with those already described in the literature (Correcher et al. 2009). Namely, four principal bands are identified, occurring at 467, 620, 791 and 1072 cm^{-1} , respectively. These bands have been conventionally assigned to:

- O–Si–O bending modes of the individual tetrahedra (467 cm^{-1});
- Si–O–Si symmetric stretching vibrations (620 and 791 cm^{-1});
- Si–O–Si asymmetric stretching vibrations (1072 cm^{-1}).

In the $2000\text{--}4000 \text{ cm}^{-1}$ region, no evidence of bands attributable to hydrated species (H_2O -, OH- stretching or bending modes) is present. Accordingly, one can thus conclude that the sample is anhydrous, within the experimental uncertainty. Moreover, in agreement with Jones and Segnit (1971), the presence of the intense band at 467 cm^{-1} is attributed to the presence of “opal-C” domains in the sample.

EPR

The room temperature cw EPR spectrum of the cristobalite sample is shown in the Fig. 3a. Apparently, only a single broad band, centred at about 300 mT, the width of which can be estimated as 100 mT, is observed. The intensity of the spectrum, estimated from the peak-to-noise ratio, is fairly low. At 35 K, the spectrum is definitely changed: almost no traces of the band observed at room temperature are

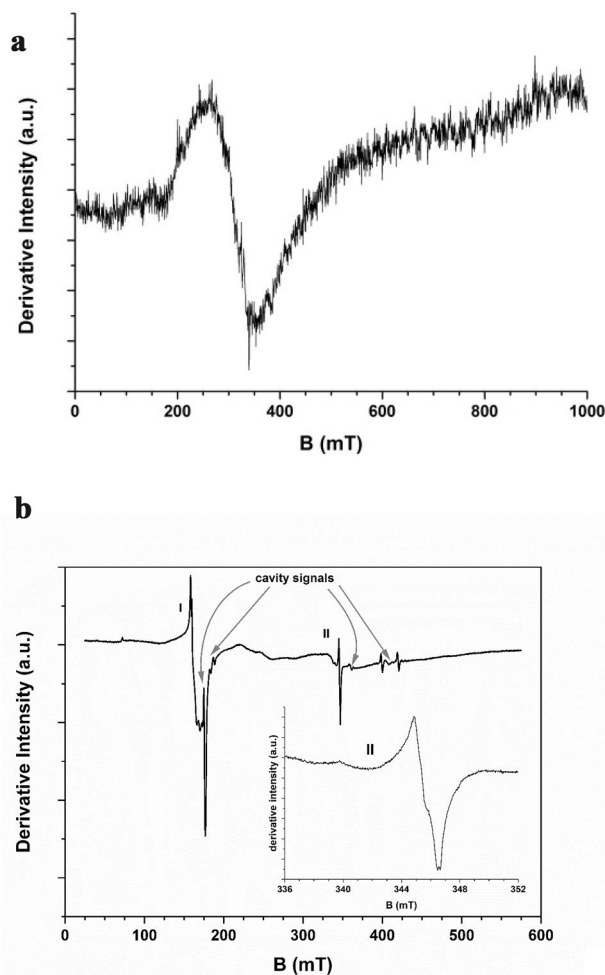


Fig. 3 cw EPR spectra of the investigated sample, registered at 298 K (a) and at 35 K (b). In the inset, detailed spectrum of the II species

detectable, whereas two additional signals are now clearly revealed: a relatively broad signal at about 160 mT (I, width about 15 mT), and a very narrow signal at 345 mT (II, width 2 mT, Fig. 3b). Both signals are clearly anisotropic. From the spectral features of the two signals, one can safely attribute the signals at 160 and 345 mT to Fe(III) ions and to radical species, respectively. Conversely, the fact that the room temperature band is no more present at 35 K supports the attribution of this band to a superparamagnetic species, such as Fe oxides/hydroxides occurring as cryptocrystalline associated phases. In these conditions, a significant shift of the band position, and, mainly, a band broadening occur (Carbone et al. 2008). The presence of Fe oxides/hydroxides, as associated mineral phases, is likely induced during the industrial synthesis of cristobalite.

The EPR spectrum of the cristobalite sample, shown in Fig. 4a, reveals the presence of only one relatively narrow and asymmetric signal, occurring at 345 mT, the width of

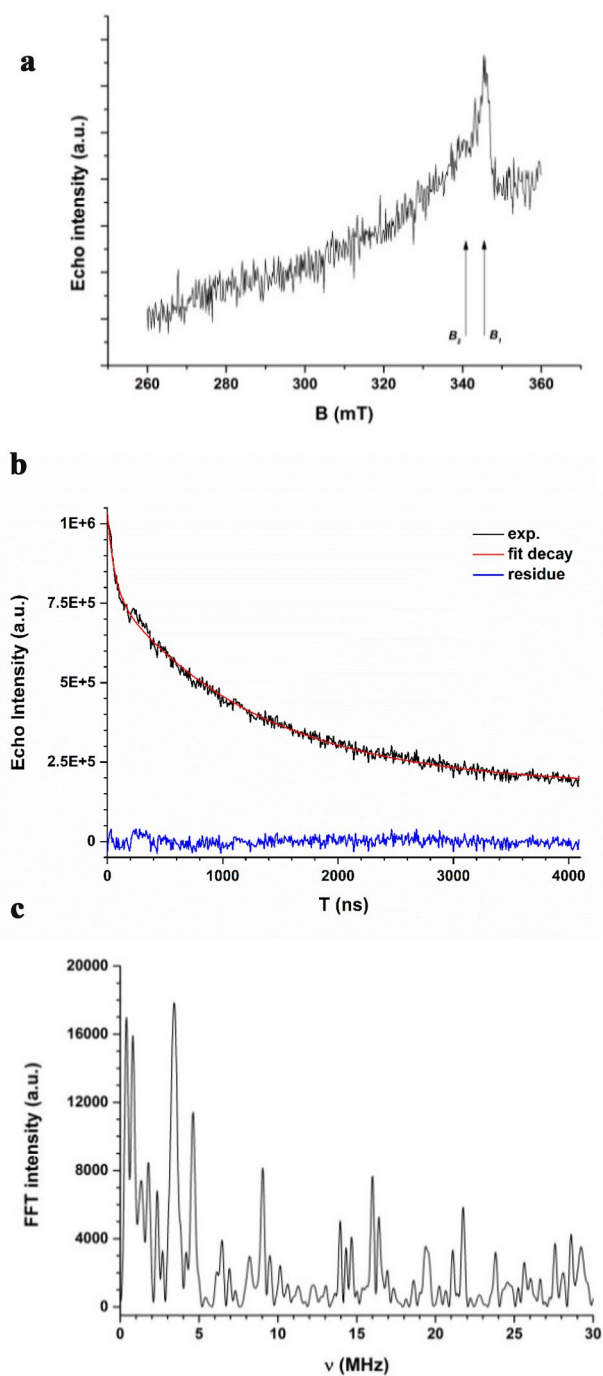


Fig. 4 Pulsed EPR spectra of the investigated sample, carried out at 35 K: **a** EEPR, **b** three-pulse decay experiments carried out at 345.7 mT, **c** Fourier Transform of the residue of the **b** spectrum after decay subtraction. Numerical modelling of the decay was accomplished using a bi-exponential function, whose best-fit parameters are: $\gamma_0 = 1.73(2) \cdot 10^6$, $A_1 = 2.38(9) \cdot 10^5$, $t_1 = 62(5)$ ns, $A_2 = 622(3) \cdot 10^5$, $t_2 = 1276(20)$ ns

which can be estimated in about 20 mT. One can tentatively attribute the most prominent peak of the signal to the inorganic radical already observed by cw EPR at 35 K, whereas

the less intense and relatively broader part of the signal can be assigned either to the parallel component of the radical species or to Cu(II) ions. A fit carried out in the assumption of two Gaussian components yields field values of 345.51(8) and 339.1(5) mT, which correspond to g values of 2.0140(5) and 2.052(3), respectively. Based on such values, the attribution of both components to the radical species appears more likely. The poor signal-to-noise ratio suggests a low abundance of the considered species.

Three pulse (3P) time-domain experiments were carried out at the magnetic field value corresponding to the maximum of the EEPR spectrum, i.e. at 345.7 mT. The experimental spectrum, shown in the Fig. 4b, exhibits a fast decay. An empirical fit of the decay behaviour, carried out by means of a multi-exponential function, yielded the best results with a bi-exponential model. The residual function (Fig. 4b), obtained after subtraction of the decay fit from the experimental raw data, points out that nuclear modulation (ESEEM) is absent. The same consideration results from the study of the FT (Fig. 4c): only very weak peaks are observed, and no peak is found whose intensity-to-noise ratio exceeds the value for the statistical significance. Thus, although some attributions to either ^{29}Si , or ^{23}Na , or ^{27}Al could be envisaged (especially considering the FT peak at ~ 3.4 MHz), a safe choice cannot be operated. This suggests that the radical has a negligible interaction with surrounding magnetic nuclei.

Discussion

Radical speciation

The EPR analysis shows a relevant contribution from radicals. Spectral simulations were performed and applied to determine the features of the Zeeman anisotropy of the radical spectrum and to contribute to its attribution. The best fit spectral simulation is shown in the Fig. 5, together with the experimental radical spectrum and the best-fit parameters.

The simulated and experimental spectra exhibit an excellent agreement. The best-fit parameters mark a rhombic asymmetry of the Zeeman tensor, with two g values (g_1 and g_2) relatively close to each other and to the free-electron value (i.e. 2.0023), whereas g_3 is definitely higher. This anisotropy could be interpreted as pseudo-axial.

Similar considerations can be fostered also concerning the anisotropic linewidth values: the best-fit parameters highlight the large value of ΔH_3 if compared with the other two values. The reference values for the Zeeman parameters of radicals associated with cristobalite samples described in the literature are listed in Table 1.

On the basis of the obtained results, our investigation suggests the attribution of the radical similar to the superoxide

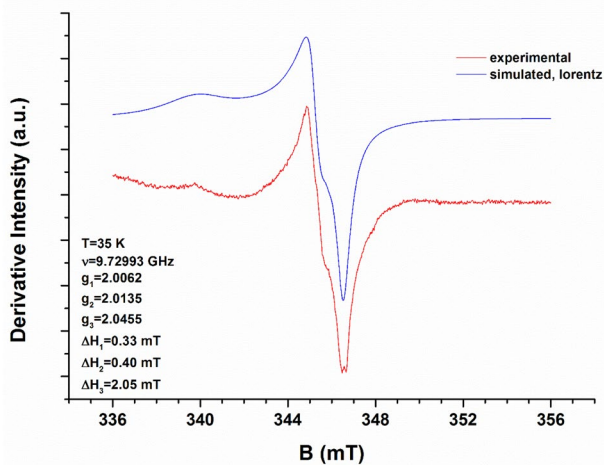


Fig. 5 Comparison between the experimental (red trace) and simulated (blue trace) spectra of the radical signal. Best-fit parameters are listed in the graph

species, like those described by Fubini et al. (1990). Our results appear also comparable to that of Giordano et al. (2007) (NBOHC, non-bridging oxygen hole center). However, the differences in the Zeeman parameters, namely for the g_3 values (2.0543 versus the present 2.0455), taking into account also the relative uncertainty in the determination of the Zeeman tensor components, suggest the attribution to NBOHC to be unlikely.

The superoxide species here invoked is characterized by the almost complete absence of protons in the surroundings, as confirmed by the 3P time-domain experiments. This fact can provide significant insight into the localization of the radical species in the sample. If the radicals would occur at the surface of the cristobalite aggregates, in fact, they would be likely interacting with protons, belonging to water molecules provided by absorption of air humidity by the sample. Conversely, if the radicals would be hosted inside the aggregates, i.e. in grain boundaries and in defect zones (as

evidenced by XRD), relatively far from their surfaces, the crystal structure itself could provide a sort of cage to prevent radical recombination and annihilation. These results are in line with the properties of the superoxide radicals studied by Fubini et al. (1990).

We are thus in favor of this localization of the superoxide radicals in the cristobalite filler sample. This attribution could also explain the unusually relevant lifetime found associated with the described radical species (repeated investigations performed after several weeks did not provide insights into the apparent decrease of radical concentration). Fubini et al. (1990) already noticed this lifetime, under laboratory conditions. These authors also described that a specific sample activation, provided by e.g. grinding, induces an increase of the radical concentration, followed by a decrease to a low, but not null, level. We want here to emphasize that the present results are obtained on industrial materials, without any kind of manipulation or pre-treatment: thus, the presence of the radical population and its specific features have to be considered as originally associated with the filler microcrystals.

Radical speciation in relation to the origin of the raw cristobalite powders and to its health effects

The combined results of the XRD, FTIR, and micromorphological characterization of the cristobalite filler microcrystalline powders reveal some interesting features that give an insight on the origin of this material. The XRPD pattern is closely resembling the characteristics of “opal C” samples (Jones and Segnit 1971; Florke et al. 1991; Curtis et al. 2019). These are materials presenting the typical features of opaline samples, with an evident but not complete crystalline organization of the cristobalite structure.

In detail, the difference between the experimental and the theoretical cristobalite patterns, mainly observed at 20–23 2θ degrees, is ascribed to the presence of highly frequent stacking disorder. The FTIR investigation carried out in the

Table 1 g tensor EPR parameters for radicals described associated with cristobalite

Name	g_1	g_2	g_3	Note	References
NBOHC	2.0025	2.0111	2.0543	hfs ^{17}O ; shfs ^{29}Si	A
E'_γ	2.0000	2.0004	2.0009	shfs ^{17}O ; hfs ^{29}Si	A
E'_2	2.0002	2.0017		hfs ^{29}Si	B
Peroxyradical	2.002	2.007	2.062		C
superoxide radical	2.002	2.010	2.044		C
Dry OHC	2.0010	2.0095	2.078		D
Wet OHC	2.0014	2.0074	2.067		D
Radical	2.0062	2.0135	2.0455		This study

OHC oxygen hole center

^AGiordano et al. (2007); ^BHochstrasser and Antonini (1972); ^CFubini et al. (1990); ^DStapelbroek et al. (1979)

present study, however, does not evidence the presence of any quantity of water, pointing to the fact that the present sample cannot be classified as opaline powders (Curtis et al. 2019).

The most striking point arising from this observation does not concern with the classification of the cristobalite filler powders but mainly deals with its origin. The described features, in fact, are not usually observed in natural cristobalite microcrystalline powders. Industrial cristobalite can be produced starting from silica sands, through a process including a silica gel formation step. According to MAK (2012) and Nurbaiti and Pratapa (2018), in fact, cristobalite can be produced by dissolution of silica precursor, followed by the formation of a silica gel by desiccation, consisting of amorphous silica powders. Then, the final cristobalite powders are obtained by calcination (at $T > 950$ °C) for several hours of the dried silica gel (the duration of the process can vary). The experimental micromorphology of the cristobalite filler of this study is indeed consistent with the micromorphology of synthetic samples obtained by gel calcination (Nurbaiti and Pratapa 2018).

We can thus conclude that the investigated cristobalite filler has a likely synthetic origin, which is the main cause of a diffuse presence of stacking disorder.

The fact that radical species are observed in a sample obtained through a high-temperature treatment suggests that the superoxide radicals were formed after this treatment. In fact, Fubini et al. (1999) demonstrated that all the known radicals associated to cristobalite are annihilated at temperature values higher than 800 °C, i.e. well below the temperature of the industrial thermal treatment (950 °C; Nurbaiti and Pratapa 2018). The radical population eventually present in the sample before calcination is thus not relevant to the present interpretation. This fact is confirmed from the absence of radiogenic h_{Al} radicals, almost ubiquitous in quartz microcrystalline powders, but also frequently described also in natural cristobalite powders.

If any original radical population has been annihilated, a question rises about the time and the process allowing the stabilization of the superoxide radical population experimentally revealed in this study. The authors suggest that superoxide radicals are formed during the heavy grinding procedures to which the materials obtained after calcination is subjected to reduce the crystal size of the particles to the very fine size here described. Moreover, the diffuse stacking disorder present in the original calcined material, and preserved and eventually increased after grinding, can be linked to the abundance of observed radicals. We do attribute the radical formation to occur preferentially in the disordered zones, where the energy associated to this process is relatively low. If radicals occurring at the surface of the aggregates are undergoing recombination according to relatively fast processes, the superoxide radicals here described, occurring

in defect regions or at grain boundaries, are somehow preserved from the recombination mechanism and remain strictly correlated to the fate of the cristobalite crystals. The main consequence of this evidence is that cristobalite powders enter any production process already activated by the presence of a certain abundance of superoxide radicals. These in turn can be let available, via airborne suspension of particles with suitable characteristics, to interaction with the workers' respiratory system.

Conclusions

The main achievement of the present study lies in the fact that an unusually abundant and stable population of superoxide radicals has been revealed and described associated to the industrial cristobalite filler powders, and likely related to the diffused stacking disorder characterizing the investigated material. We point out that the specific formation of the superoxide radical population is to be attributed to the formation of the cristobalite microcrystalline powders: namely, the high-temperature calcination from a gel precursor state provides the diffuse structural disorder, which, in turn, favours the formation and stabilization of the radicals during a successive grinding step (necessary to achieve powders of the correct granulometry for the final industrial use). The specificity of this formation of radicals and their intrinsic stability provide a peculiar case in the field of the studies of radicals associated with crystalline silica. Indeed, their presence was never described in previous studies concerning industrial raw materials (Romanelli et al 2012; Di Benedetto et al 2019). This fact and the long endurance of the superoxide radical population are unlikely a general property of radicals associated with crystalline silica materials used in industrial settings. Accordingly, we foster this feature as highly interesting for relationships to the health and toxicology implications. Further studies, aimed at assessing the toxicological effects of this material, are in progress. The present results appear linked to the experimental evidences that suspect a higher toxic potential for cristobalite than for α -quartz. The limited epidemiological confirmation of such differential toxicity is poorly discussed mainly because few cohorts of workers were specifically found exposed to relevant amounts of respirable dusts of cristobalite (e.g. the workers of the diatomite industry; Park et al. 2002). However, the recent activation of new processes where cristobalite dust could be a frequent and relevant raw material deserves renewed attention to this task.

Acknowledgements The authors are indebted to L. Chelazzi, L. Chirantini, T. Salvatici for their assistance during the XRD, SEM/EDX, and FTIR measurements, respectively.

Author contributions The manuscript was written through the contributions of all authors. All authors have given approval to the final version of the manuscript.

Funding Open Access funding provided by Università degli Studi di Firenze. This study was funded by University of Florence (Fondi di Ateneo 2018, 2019) and by INAIL under the program “Studio su rischi e fattori di rischio noti ed emergenti per la individuazione e prevenzioni di tumori professionali”.

Compliance with ethical standards

Conflict of interest There are no competing interests.

Open Access This article is licensed under a Creative Commons Attribution 4.0 International License, which permits use, sharing, adaptation, distribution and reproduction in any medium or format, as long as you give appropriate credit to the original author(s) and the source, provide a link to the Creative Commons licence, and indicate if changes were made. The images or other third party material in this article are included in the article's Creative Commons licence, unless indicated otherwise in a credit line to the material. If material is not included in the article's Creative Commons licence and your intended use is not permitted by statutory regulation or exceeds the permitted use, you will need to obtain permission directly from the copyright holder. To view a copy of this licence, visit <http://creativecommons.org/licenses/by/4.0/>.

References

- ACGIH (2010) Silica, crystalline: alpha-quartz and cristobalite: TLV(R). In: Chemical Substances 7th Edition Documentation, pp 18
- Altomare A, Corriero N, Cuocci C, Falcicchio A, Moliterni A, Rizzi R (2015) QUALX2.0: a qualitative phase analysis software using the freely available database POW_COD. *J Appl Cryst* 48:598–603
- Andersson L, Bryngelsson I-L, Ohlson C-G, Nayström P, Lilja B-G, Westberg H (2008) Quartz and dust exposure in Swedish iron foundries. *J Occ Environ Hyg* 6(1):9–18. <https://doi.org/10.1080/15459620802523943>
- Barbieri PG, Somigliana A, Carradori G (2020) Severe silicosis due to diatomaceous earth in dental alginate: a necropsy study. *Work Environ Health* 3:222–231 (in Italian)
- Carbone C, Di Benedetto F, Sangregorio C, Marescotti P, Pardi LA, Sorace L (2008) Multifrequency EMR and magnetic characterization of synthetic powdered hematite. *J Phys Chem C* 112:9988–9995
- Correcher V, Garcia-Guinea J, Bustillo MA, Garcia R (2009) Study of the thermoluminescence emission of a natural cristobalite. *Rad Effects Defects Solids* 164(1):59–67
- Curtis NJ, Gascooke JR, Johnston MR, Pring A (2019) A review of the classification of opal with reference to recent new localities. *Minerals* 9:299–1–20. <https://doi.org/10.3390/min9050299>
- Daniel LN, Mao Y, Wang TC, Markey CJ, Markey SP, Shi X, Saffiotti U (1995) DNA strand breakage, thymine glycol production, and hydroxyl radical generation induced by different samples of crystalline silica in vitro. *Environ Res* 71(1):60–73
- Di Benedetto F, Giaccherini A, Montegrossi G, Pardi LA, Zoleo A, Capolupo F, Innocenti M, Lepore GO, d'Acapito F, Capacci F, Poli C, Iaia TE, Bucciati A, Romanelli M (2019) Chemical variability of artificial stone powders in relation to their health effects. *Sci Rep* 9:6531. <https://doi.org/10.1038/s41598-019-42238-2>
- Florke OW, Graetsch H, Martin B, Röller K, Wirth R (1991) Nomenclature of micro- and non-crystalline silica minerals, based on structure and microstructure. *N Jb Miner Abh* 163(1):19–42
- Fubini B, Giamello E, Volante M, Bolis V (1990) Chemical functionalities at the silica surface determining its reactivity when inhaled. Formation and reactivity of surface radicals. *Toxicol Ind Health* 6(6): 571–598
- Fubini B, Zanetti G, Altilia S, Tiozzo R, Lison D, Saffiotti U (1999) Relationship between surface properties and cellular responses to crystalline silica: studies with heat-treated cristobalite. *Chem Res Toxicol* 12:737–745
- Giordano L, Sushko PV, Pacchioni G, Shluger AL (2007) Optical and EPR properties of point defects at a crystalline silica surface: ab initio embedded-cluster calculations. *Phys Rev B* 75:024109-1–24119
- Hochstrasser G, Antonini JF (1972) Surface states of pristine silica surfaces I. ESR studies of E_s[•] dangling bonds and of CO₂⁻ adsorbed radicals. *Surf Sci* 32:644–664
- Horwell CJ, Fenoglio I, Ragnarsdottir KV, Sparks RSJ, Fubini B (2003) Surface reactivity of volcanic ash from the eruption of Soufrière Hills volcano, Montserrat, West Indies, with implications for health hazards. *Environ Res* 93:202–215
- IARC, International Agency for Research on Cancer (2012) A review of human carcinogens: arsenic, metals, fibres, and dusts. In: IARC Monographs on the evaluation of carcinogenic risks to humans 100C, IARC, Lyon, France
- Jones JB, Segnit ER (1971) The nature of opal I. nomenclature and constituent phases. *J Geol Soc Australia: Int Geosci J* 18(1):57–68
- Leso V, Fontana L, Romano R, Gervetti P, Iavicoli I (2019) Artificial stone associated silicosis: a systematic review. *Int J Environ Res Public Health* 16:568. <https://doi.org/10.3390/ijerph16040568>
- MAK Value Documentation (2012) Silica, crystalline: quartz dust, cristobalite dust and tridymite dust (respirable fraction). <https://doi.org/10.1002/3527600418.mb0sio2fste0014>
- Murgia N, Muzi G, Dell'Omo M, Sallèse D, Ciccotosto C, Rossi M, Scatolini P, Zingarelli A, Accattoli MP, Melchiorri D, Abbritti G (2007) An old threat in a new setting: High prevalence of silicosis among jewelry workers. *Am J Ind Med* 50(8):577–83. <https://doi.org/10.1002/ajim.20490>
- Musso F, Ugliengo P, Solans-Monfort X, Sodupe M (2010) Periodic DFT study of radical species on crystalline silica surfaces. *J Phys Chem C* 114:16430–16438
- Nurbaiti U, Pratapa S (2018) Synthesis of cristobalite from silica sands of Tuban and Tanah Laut. *J Phys Conf Ser* 983:012014
- Park R, Rice F, Stayner L, Smith R, Gilbert S, Checkoway H (2002) Exposure to crystalline silica, silicosis and lung disease other than cancer in diatomaceous earth industry workers: a quantitative risk assessment. *Occup Environ Med* 56:36–43
- Romanelli M, Di Benedetto F, Bartali L, Innocenti M, Fornaciai G, Montegrossi G, Pardi LA, Zoleo A, Capacci F (2012) ESEEM of industrial quartz powders: insights into crystal chemistry of Al defects. *Phys Chem Min* 39:479–490
- Stapelbroek M, Griscom DL, Friebele EJ, Sigel GH Jr (1979) Oxygen-associated trapped-hole centers in high-purity fused silicas. *J Non Cryst Sol* 32:313–326
- Sugiyama Y, Tamure M, Ikari A (1998) Electron spin resonance studies on spots with brown rims on a vitreous silica surface formed by a silicon melt. *Jpn J Appl Phys* 37:6390–6393
- USGS, U.S. Geological Survey (2016) Minerals yearbook silica [advance release] 66.1–66.15, 2016, <https://prd-wret.s3-us-west-2.amazonaws.com/assets/palladium/production/atoms/files/myb1-2016-silic.pdf>. Accessed the 10/10/19

Publisher's Note Springer Nature remains neutral with regard to jurisdictional claims in published maps and institutional affiliations.